Holographic Vibration Measurement of a Rotating Fluttering Fan

Philip A Storey*
Rolls-Royce Limited, Derby, England

The use of holographic interferometry to determine the deflection shape of a rotating aero engine fan undergoing unstalled supersonic flutter is described. A mirror-Abbé image rotator was employed in a double pulse holographic system to compensate for the fan's rotational motion and thus maintain correlation between the two resultant holographic images. The mirror-Abbé unit both rotated the illuminating beam and derotated the light returned from the rotating fan. Holographic interferograms were recorded of a 0.86-m-diam fan rotating at speeds just under 10,000 rpm and undergoing unstalled flutter. The amplitude and spatial distribution of blade torsion and axial bending on the fluttering fan are obtained from the holograms. Errors due to misalignment of the system and unsteady aerodynamics are discussed.

Introduction

AEROELASTIC instability is often a constraint on the design of modern high-bypass-ratio aero engines. Unstalled supersonic flutter is an instability that can be encountered in clappered (shrouded) fans, in which mechanical vibrations give rise to unsteady aerodynamic forces that couple further energy into the mechanical vibration. This phenomenon is particularly sensitive to the deflection shape of the mechanical vibration. Successful computation of the flutter onset conditions is similarly sensitive to this deflection shape. This paper describes the first reported use of holographic interferometry to determine the deflection shape of a rotating fan undergoing unstalled flutter.

Conventional measuring techniques, such as strain-gages and accelerometers attached to the fan blades and overtip proximity transducers housed in the fan casing, provide information about the deflection shape of a rotating fluttering fan at only a limited number of positions. Holographic interferometry allows the determination of an object's vibration deflection over its full visible surface. This feature has led to the use of the technique for modal analysis of non-rotating bladed-disk assemblies.[1,2]

The use of holographic interferometry to study the vibration of rotating structures often requires some form of rotation compensation. In the case of double-exposure holography, this is a requirement where the rotational movement is greater than the mean speckle size in the holographic image, otherwise decorrelation between the two images results in loss of fringe visibilty.

Historically, several methods have been proposed and tested to prevent image decorrelation due to object rotation, and they fall into three basic categories. The first category consists of techniques in which two states of the object having the same angular position are compared interferometrically. Several reports have been made in which a rotating object has been compared holographically with its static state.[3,4] These techniques are limited to measurement of only small deflections, typically much less than 100 μm, and are thus not suitable for determination of the much larger deformations found in unstalled fan flutter. The second approach is that of rotating the holographic recording material at the same speed as the object. This is achieved by attaching the recording film or plate to the object[5,6] or, alternatively, by rotating it using a separate shaft.[7] Both alternatives are fraught with practical difficulties for remote rig running. The third approach is to use an image rotator, synchronized to half the speed of the rotating object, to optically compensate for its motion.[8-16] The third method is the most easily applied to an aero engine fan in a test facility environment, and this is the approach adopted herein for fan flutter measurements. A review of this subject is given by MacBain.[17]

This paper describes the design and special features of a holographic system employing a mirror-Abbé image rotator for measuring the axial component of vibration of a rotating fan. The use of the system to obtain holographic interferograms of a fluttering fan and the analysis of those interferograms is described. Some sample results which quantify the distribution of the axial deflection of the fluttering fan are then presented.

Image Rotator

Most image rotators fall into one of two categories,[18] either transmissive or reflective. Holographic systems employing both types have been reported. Stetson's pioneering system[8,9] used a transmissive folded-Abbé rotator. This is the only previously reported holographic system that has been applied to the measurement of vibration of rotating aero engine fans. Interferograms obtained with this system of a 0.81-m-diam fan operating at speeds up to 7500 rpm were reported. More recently, a reflective Porro prism rotator has been used by Beeck et. al[15,16] in a holographic system for measurements on a 0.43-m-diam automobile cooling fan at reported speeds up to 2850 rpm. This system has also been used on a 0.25-m-diam disk at speeds up to 13000 rpm.

The author decided upon a transmissive image rotator because this simplified the holographic system and minimized the required number of passes of the object beam through a beam splitter, thus also minimizing the attendant loss of light. A mirror-Abbé rotator configuration, as shown in Fig. 1, was chosen. This is the simplest collinear transmissive rotator, having the whole of the optical path in air, thus making the rotator free from unwanted back-reflections and aberrations. These features, together with the use of dielectric mirror coatings, allow rotation of the high intensity illuminating beam as well as derotation of the returned scattered light from the fan. The ability to rotate the illuminating beam increases the versatility of the holographic system, as described in the following section. The mirror-Abbé configuration does have a

Presented as Paper 82-1271 at the AIAA/SAE/ASME 18th Joint Propulsion Conference, Cleveland, Ohio, June 21-23, 1982; submitted June 25, 1982; revision received Jan. 11, 1983.

*Research Scientist, Advanced Research Laboratory.

high inertia due to its off-axis mirror, thus making very high speed operation difficult. However, a 27 mm aperture unit capable of operation at object speeds up to 12,000 rpm has been built, as described below. This speed capability is adequate for most aero engine fan applications.

The mirror-Abbé optics are formed from two optical elements; a glass prism forms the two on-axis mirrors and a separate, off-axis mirror is used. These are mounted in a steel housing that is held on the axis of a modified Vatric-Mavilor 600 dc motor. This has a light, ironless, dish-shaped armature that gives low inertia, near constant torque from rest to high speeds and a high power to length ratio. The motor was modified to produce a hollow shaft of 30 mm i.d. A section through the image rotator is shown in Fig. 2. The rotor assembly is supported in externally pressurized air bearings; two journal bearings and a double-acting thrust bearing. Air bearings are used because of their good centering properties, smooth running, and low vibration. An optical tachometer is incorporated that provides 120 pulses per revolution (ppr) and 1ppr outputs. This rigid rotor assembly was dynamically balanced at high speed using accelerometers in two planes and an influence coefficient method.[19] The unit is shown in Fig. 3.

The image rotator is synchronized at half the object speed using a phase-locked loop control system that enables the rotator to follow fluctuations in object speed. A simplified block diagram of the control system is shown in Fig. 4. The phase comparator compares the phase of a 60 ppr tachometer signal from the object with that of the 120 ppr signal from the rotator, and gives an output that is a measure of the phase difference between these two inputs. This difference signal is filtered, amplified, and then used to drive the motor. The motor control voltage changes the motor speed in a direction that reduces the phase difference between the two tachometer signals. When the loop is "locked," the motor control voltage is such that for every object tachometer pulse there is one, and only one, tachometer pulse from the rotator, thus ensuring that the rotator is maintained at exactly half the speed of the object.

During the acquisition of "lock" there are large voltage swings at the output of the phase comparator. Thus, saturation of the amplifier is prevented by using a low amplifier gain during lock acquisition. Once lock has been obtained, the gain of the amplifier is automatically increased so as to maximize the speed range over which lock can be held (hold range).

The filter was designed to produce a control loop having second-order characteristics and lag-lead compensation. This allowed the independent selection of loop gain, bandwidth, and damping, producing a control system having a reasonable tracking range, a bandwidth sufficient to follow fan speed fluctuations, good transient response, and good noise rejection properties. The tracking performance of the control system, together with a summary of the mechanical and optical characteristics of the rotator, is given in Table 1.

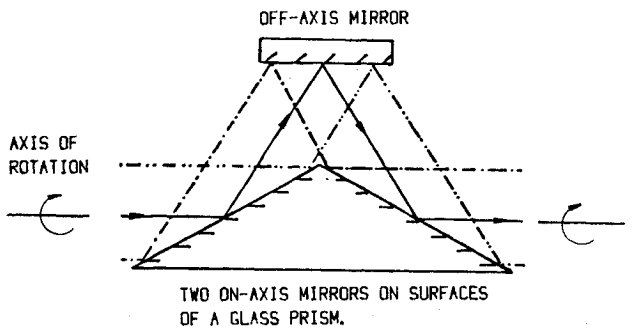

Fig. 1 The mirror Abbé image rotator.

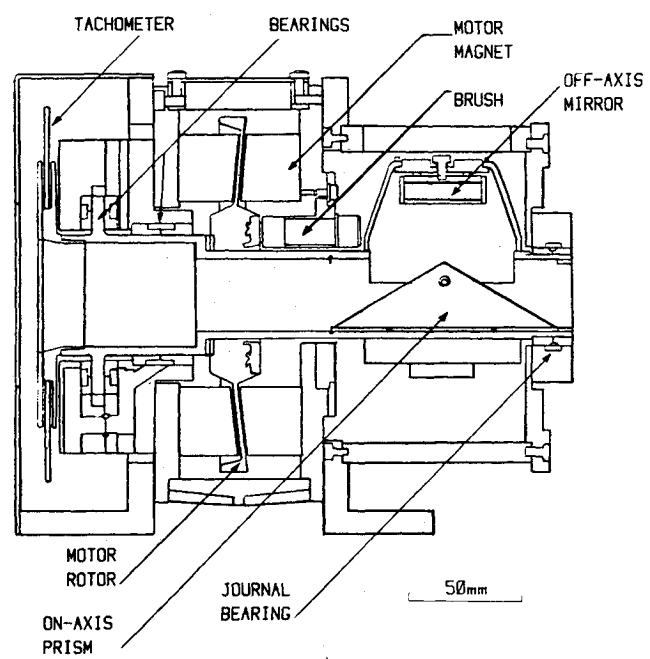

Fig. 2 Diagram of a section through the image rotator.

Holographic System

A diagram of the optical system is shown in Fig. 5. The image rotator both rotates the illuminating object beam and derotates the light scattered from the fan before it is relayed

Table 1 Mechanical, optical and control characteristics of the rotator

Parameter	Value
Maximum object speed, rpm	12,000
Optical *f* number	7.2
Optical aperture diameter, mm	27
Hold range,[a] rpm	800
Maximum peak-to-peak variation in object speed at 1Hz before drop out,[b] rpm	300
Maximum peak to peak variation in object speed at 10Hz before drop out,[b] rpm	150

[a] Hold range is the range of fan speed over which lock is maintained, having once set a center speed. [b] These figures show the capability of the control system to maintain "lock" when presented with a sinusoidally varying fan speed.

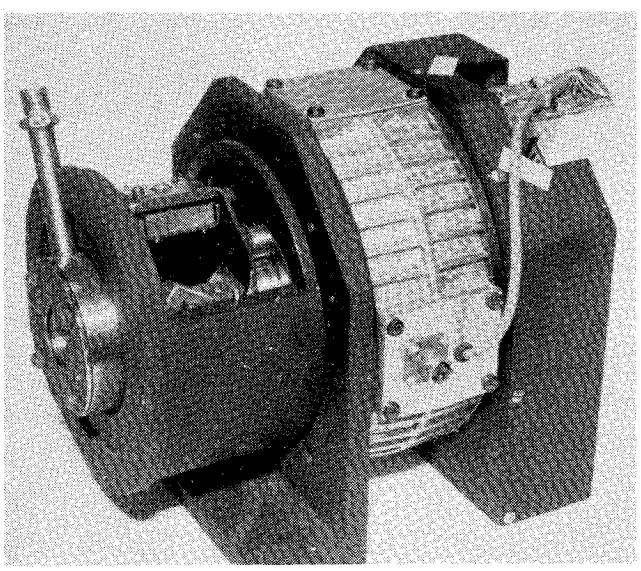

Fig. 3 Photograph of the mirror Abbé image rotator.

onto the hologram recording plane. This overcomes the decorrelation between the two holographic images that would otherwise be present. The use of rotating illumination relaxes the tolerance on the spatial quality and alignment of the illuminating beam and even allows the use of diffuse illumination. It allows the available laser light to be concentrated into an off-axis position of the fan, and when used in this mode, there is the operational convenience of being able to rotate the illuminated area on the fan by simply phase locking the image rotator at a different orientation with respect to the fan.

The viewing and illumination are from a point on the fan's projected rotational axis, thus ensuring that the holographic sensitivity vector is orthogonal to the fan rotation. This prevents unwanted optical path-length variation due to fan rotation, which would produce distorting bias fringes in the resultant holographic interferogram. The need for othogonality of the sensitivity vector and the fan's rotation limits the technique to the measurement of only the axial component of fan vibration. The fine adjustment of the optical system relative to the fan's rotational axis is performed using two alignment mirrors, positioned between the image rotator and the fan.

Apart from the above features, the optical configuration is that of a conventional double-pulse holographic system. A Q-switched pulsed ruby laser giving up to 0.5 J in two 25 ns duration pulses is used. The pulse separation is variable from 2 μs to several hundred microseconds. The laser operates at a wavelength of 0.694 μm and reliably produces a coherence length in excess of 0.7 m, which corresponds to no more than two adjacent longitudinal modes.[20] This coherence is adequate for the generation of holograms of fans that are several meters in diameter.

The laser output is divided at a wedged beamsplitter where 4% of the light is reflected to produce a reference beam. The majority of the light forms the object beam. This is projected through the image rotator onto the fan using illumination optics and a 50% beamsplitter. Where a large angle of illumination, approaching the full angle of view of the image rotator, is required, the illumination optics consist of a diverging lens, a weak diffuser, and a converging lens, as shown in Fig. 5. The two lenses focus the beam within the rotator, and the diffuser prevents air breakdown by reducing the beam intensity at the focus. When a smaller angle of illumination is required, such as when the available light is concentrated into an off-axis portion of the fan, the illumination optics simply consist of a negative lens that diverges the beam through the rotator onto the fan.

The hologram is recorded using either thermoplastic film or a conventional silver halide film such as Agfa 10E75. The thermoplastic recording is performed using a Rottenkolber camera, model HSB100, and film type PT100. The use of thermoplastic film allows the holographic interferogram to be viewed remotely only a few seconds after recording. This is achieved by employing a video camera to view the holographic image and a reconstruction system using a helium-neon laser and remotely operable shutter.

The relay optics between the image rotator and the hologram recording film are used to match the angular spread of the returned light to the spatial frequency characteristics of the film, thus maximizing the energy density at the film. None of the spherical optics, either associated with fan illumination or relaying the image to the film, appears on the same side of the rotator as the fan, as this would have demanded fine manufacturing and positional tolerances of any such components.

A triggering system is used that ensures that the laser pulses occur at a coincidence of selected points in the fan's rotational cycle and the vibrational cycle. A once-per-revolution fan signal and the output from a strain-gage on the fan are used as inputs to the triggering system. The triggering system not only provides a pulse that Q-switches the laser at the required coincidence, but also predicts this coincidence, approximately 1ms before it occurs, and provides a pulse that fires the laser flash tubes. This prediction is performed assuming constant rotational velocity and vibration frequency.

The holographic system is housed in a compact two-tier frame, with the ruby laser mounted on the lower level and the rest of the optical system on the upper level. The complete frame is mounted on screw-jacks, thus providing a coarse vertical adjustment on the position of the optical axis of the system. The approximate size of the unit is 1.3 m long, 1 m wide, and 1.2 m high.

Alignment Procedure

The fan's projected axis must pass through the center of the rotator aperture in order to prevent unwanted bias fringes on the resultant interferogram due to fan rotation. This fine alignment is performed using two output alignment mirrors. The relative angle between the fan and rotator axes is changed by adjustment of two orthogonal tilt controls, and the relative displacement between these axes is adjusted by means of vertical and horizontal displacement controls. The optical axis of the rotator is made closely collinear with the rotational axis of the fan, as determined at very low speed. This alignment is performed as follows, using the configuration shown

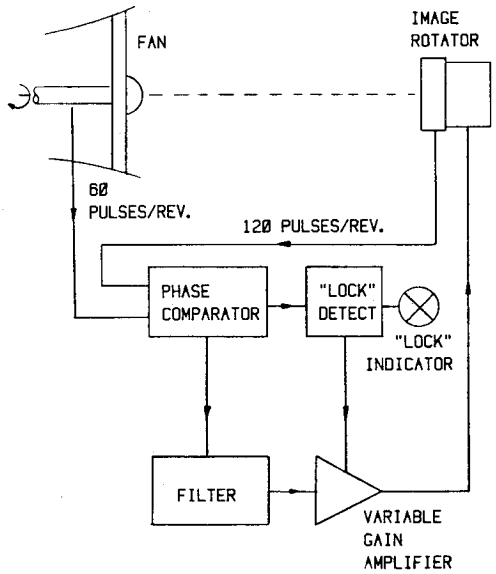

Fig. 4 The phase-locked loop control system.

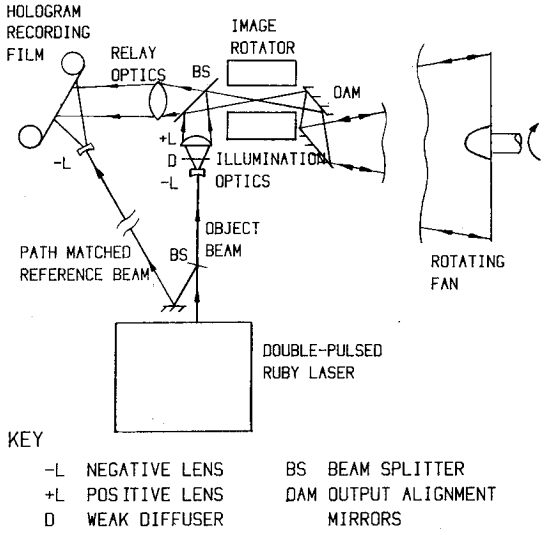

Fig. 5 The holographic system.

schematically in Fig. 6:

1) A slightly converging helium-neon laser beam is aligned to the optical axis of the spinning rotator by adjustment of mirrors A and B. This is achieved when the loci defined by the rotating beam in the near and far field of the output of the rotator are spots of minimum diameter.

2) A small, adjustable mirror, C, attached to the center of the fan, is aligned normal to the fan's rotational axis. This is obtained by monitoring the locus of a reflected laser beam at a distant screen while the fan is slowly rotated by hand.

3) The output alignment mirrors are then adjusted such that the beam aligned to the axis of the rotator is incident on the center of the fan and is collinear with the resultant reflected beam.

4) Mirrors A, B, and C are then removed and the holographic system is reassembled.

Following this procedure, the projected fan axis is typically within ± 3 mm of the center of the rotator apertures.

Laboratory Trials

The holographic system was used to record interferograms of a 0.56-m (22-in.) -diam clappered fan. The fan was rotated in a vacuum chamber and viewed through a large glass window. Individual modes of vibration of the fan could be excited using piezoelectric crystal exciters that were attached to the fan blades and powered via a slip ring unit. This fan rig proved to be an excellent laboratory facility for development of the holographic system. An example of the interferograms obtained is shown in Fig. 7. This was recorded using a pulse separation of 18 μs with the fan rotating at 4125 rpm and vibrating predominantly in a second family assembly mode having two diametral nodes (2D2F).

Investigation of a Fluttering Fan

The holographic system was used to measure the axial vibration shape of a fan undergoing supersonic unstalled flutter. The fan was 0.86 m (34 in.) in diameter and was installed in an air-turbine-driven compressor test rig. The test rig had a variable choke core section and a separate bypass section. A flared intake, open to the atmosphere, was employed for these measurements. The instrumentation included strain-gages on six of the fan blades. The fan was sprayed with retro-reflective paint in order to increase greatly the light returned to the holographic system.

The holographic unit was mounted on axis, 6 m in front of the fan, as shown in Fig. 8. The available laser light was directed onto approximately one quarter of the area of the fan, so as to increase the object beam intensity at the hologram recording plane. Holograms were recorded on Agfa Gevaert 10E75 film, using a remotely operated film transport system. It was originally intended to use thermoplastic film, which would have allowed remote viewing of the interferograms, but unfortunately a fault developed in this system during the early stages of the test. The reference beam was folded within the two-tier optics unit to give an optical path of 12-m, thus path matching the object beam. Full remote control of the system was employed, including control of all of the important laser parameters, the image rotator, and the film transport. Up to 70 holograms were recorded before a film change became necessary.

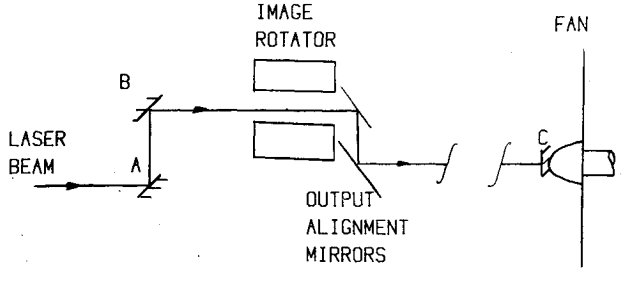

Fig. 6 Configuration used for alignment.

Approximately 100 useful holograms were obtained during 6 h of running over a 2 day period. The majority of these were recorded with the fan in steady unstalled flutter, at speeds just below 10,000 rpm and with a flutter frequency of 686 Hz. Holograms were recorded at selected fan orientations and alternating stress levels and at various phases in the flutter cycle. The interferograms showed the fan to be fluttering with a 3D2F mode shape with a peak velocity of the order of 1 ms^{-1}. Two examples of the interferograms recorded in flutter are shown in Figs. 9 and 10. They were recorded at fan speeds of 9890 and 9886 rpm, respectively, using a pulse separation of 2 μs. The holograms were recorded at approximately the same fan orientation, but at different phases with respect to the flutter cycle. The change in the circumferential orientation of the fringe pattern shows the traveling nature of the flutter vibration. A few interferograms were recorded at fan speeds just below the onset of flutter. An example is shown in Fig. 11, which was recorded at a fan speed of 9664 rpm and with a pulse separation of 9 μs. It can be seen that out of unstalled flutter there is significant vibrational activity of individual blades, particularly at the leading edge, with vibrational velocities of the order of 0.3 ms^{-1}. A similar individual blade response superimposed on the 3D2F mode shape can be seen on many of the interferograms recorded in flutter.

The holographic results were obtained with the fan operating with a wide-open bypass throttle to give the lowest flutter speed. The use of retro-reflecting paint affected the aerodynamic and flutter performance of the fan. The total flow and the flutter onset were reduced by 4.5% and 6%, respectively. This is likely to be due to an increase in the blade surface roughness from approximately 30 to 250 μ in. CLA and a thickening of the leading edge of the blades, as a result of the application of the paint. Even though there was a significant change in the fan's characteristics, the holographic measurements are of use for comparison with the predicted mode shape, as determined by finite element techniques, and for study of the fundamentals of the flutter process.

Estimate of Errors in Fringe Position

In addition to the errors present in conventional holographic interferometry, such as those incurred in determining

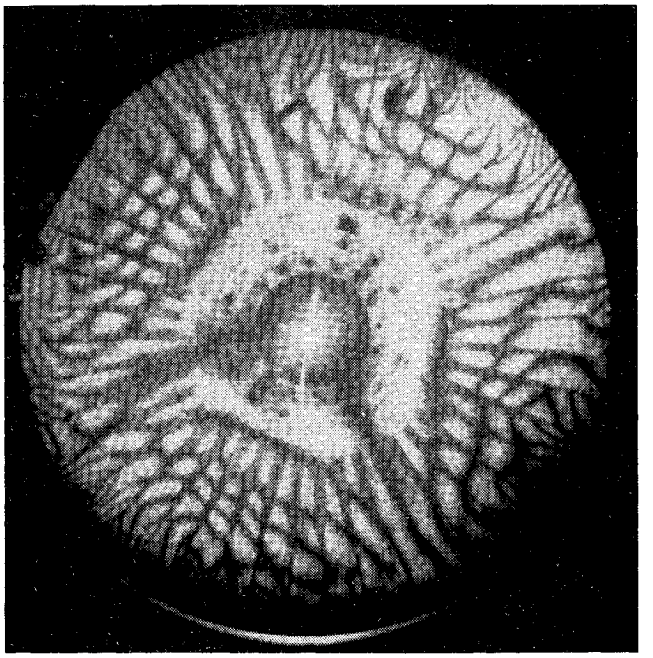

Fig. 7 Interferogram of fan rotating at 4125 rpm and vibrating predominantly in a 2D2F mode.

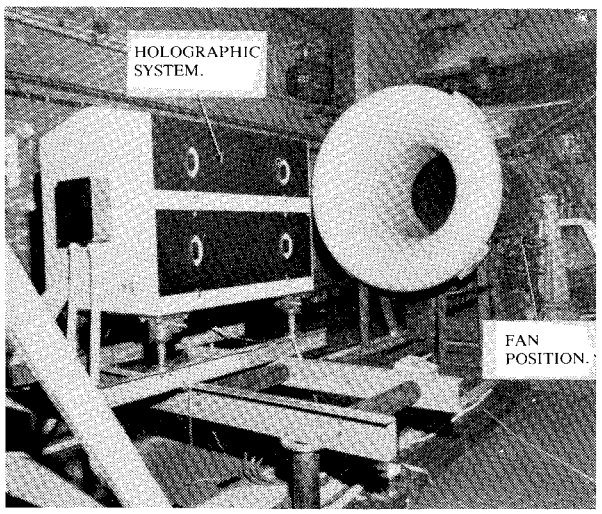

Fig. 8 The holographic system mounted in the compressor test facility prior to taking measurements in flutter.

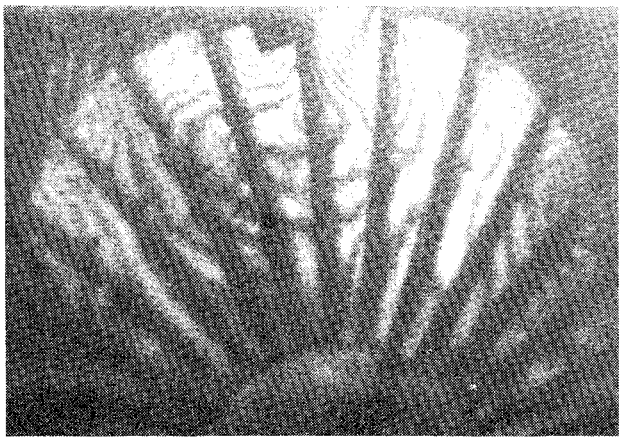

Fig. 9 Interferogram of the fluttering fan, obtained at a fan speed of 9890 rpm.

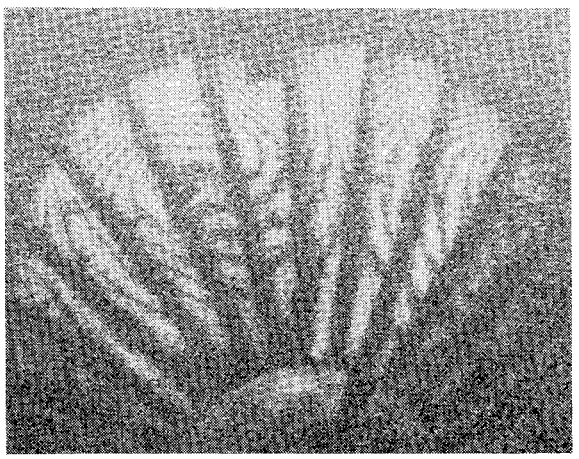

Fig. 10 Interferogram of the fluttering fan, obtained at a fan speed of 9888 rpm.

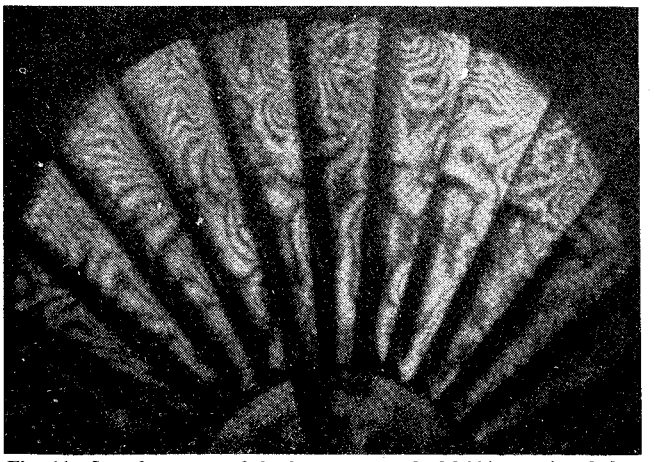

Fig. 11 Interferogram of the fan, at a speed of 9664 rpm, just below the onset of flutter.

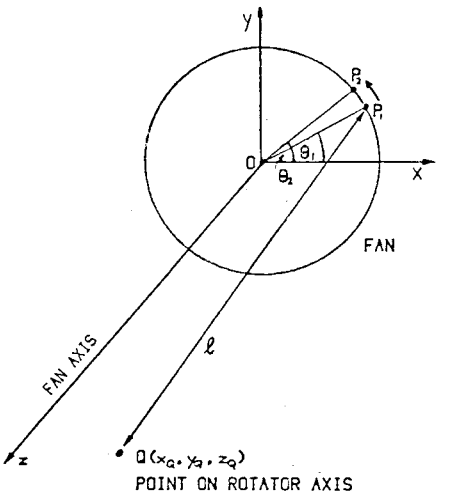

Fig. 12 Geometrical configuration used for the calculation of bias fringes.

the precise position of a fringe and its order, there are two further sources of error worthy of consideration for the case of a rotating fan under aerodynamic load. These sources of error are discussed next. First, the effects of misalignment of the holographic system relative to the rotational axis of the fan are quantified, and second, the path-length changes due to unsteady aerodynamics are considered.

The holographic system is optically aligned when the projected fan's axis passes through the center of the image rotator apertures. In this condition, the holographic sensitivity vector is perpendicular to the fan's direction of rotation at all points, and thus no biasing of the interference fringes occurs due to rotation. When this is not the case, the fringe order at each point on the fan is modified according to the relationship

$$m = (2\Delta\theta/\lambda\ell)\ (x_p y_Q - y_p x_Q) \tag{1}$$

where m is the change in the fringe order at a point p on the fan due to misalignment, λ is the wavelength of light, $\Delta\theta$ the angle of rotation occuring between exposures, ℓ is the distance between the rotator and point p, x_p and y_p the coordinates of a point p on the fan, and x_Q and y_Q are the coordinates of a point Q on the rotator axis as defined in Fig. 12.

Equation (1) is derived in the Appendix for point illumination and observation at point Q on the image rotator axis. For the case where the fan to image rotator distance is large compared with the fan radius, ℓ is approximately constant for all points on the fan and the change in the fringe distribution can be approximated by a set of parallel equispaced bias fringes.

The likely errors in the flutter measurements due to misalignment are now considered. When installing the holographic system it was estimated that the center of the image rotator apertures was aligned to within ± 3 mm of the projected axis of the static fan. Prior measurements suggested that movement of the fan's axis between static and full speed conditions was minimal compared with the installation error. Thus, by substituting into Eq. (1) the appropriate values for holograms recorded at a fan speed of 10,000 rpm, a pulse

separation of 2 μs, and a 3 mm misalignment, the maximum error in the fringe order is determined as 1.2 full fringes. This worst error condition would occur at the tips of two diametrically opposite blades.

Unsteady aerodynamics, and in particular a moving intrapassage shock, will produce some biasing of the interference fringe distribution. The magnitude of that biasing is now estimated. The change in the fringe order resulting from a movement of the shock is given by:

$$\Delta F = (Cd/\lambda)\ (\rho_2 - \rho_1) \tag{2}$$

where ΔF is the change in the fringe order, due to shock movement; C the Gladstone-Dale constant, equaling 2.24×10^{-4} m^3 kg^{-1} for air; d the total optical path length over which the shock moves between exposures; and ρ_1 and ρ_2 are the pre- and post-shock air densities, respectively.

A normal shock moving with an amplitude a at a flutter frequency ω, as shown in Fig. 13, is considered. For pulse separations, Δt, short compared with the flutter cycle time, the maximum shock movement occurring between exposures is $\omega a \Delta t$. Thus, the maximum value of d is given by

$$d = 2\omega a \Delta t \sec(\delta) \tag{3}$$

where δ is the blade stagger angle, and the factor 2 has been included because a double-pass optical system is used. Thus from Eqs. (2) and (3) we obtain,

$$\Delta F = [2C\omega a \Delta t \sec(\delta)]\ (\rho_2 - \rho_1)/\lambda \tag{4}$$

An estimate of the change in the fringe order due to unsteady aerodynamics can now be made by substituting appropriate values into Eq. 4. A change in the fringe order of approximately 0.01 of a full fringe is predicted for the following estimated typical conditons; $\omega = 4310$ rad s^{-1}, $a = 1$mm, $t = 2\mu$s, $\delta = 60$ deg, $(\rho_2 - \rho_1) = 1$ kgm^{-3} and $\lambda = 0.694\ \mu$m.

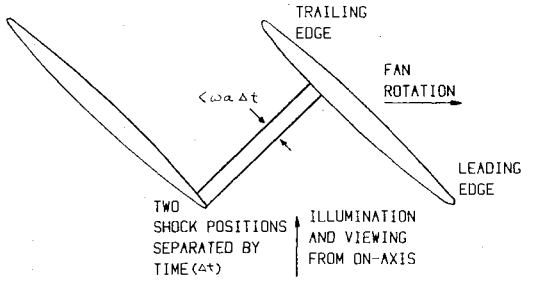

Fig. 13 Model used to calculate errors due to unsteady aerodynamics.

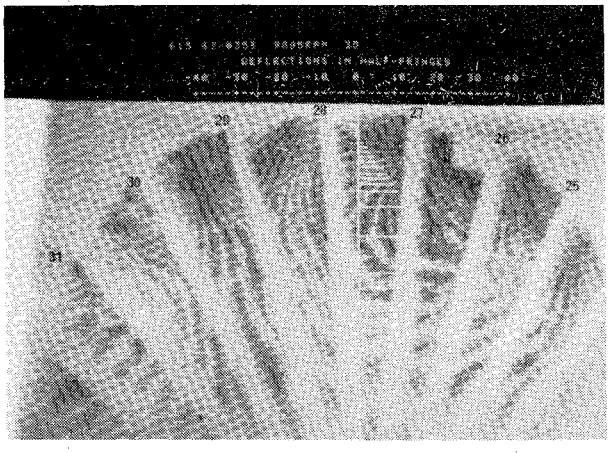

Fig. 14 Interferogram of the fluttering fan, recorded from the visual display of the analysis system.

Thus, careful alignment of the holographic system relative to the rotational axis of the fan is very important in minimizing the errors in the resultant deflection data. Errors due to unsteady aerodynamics are typically much smaller.

Quantitative Analysis of the Interferograms

The interferograms were analyzed to obtain the axial component of the flutter vibration shape, with particular emphasis on determining the spatial distribution and relative magnitudes of axial displacement and torsion of the blades. The distribution of blade torsion and displacement is important for modeling and prediction of the unstalled flutter phenomenon. The analysis was performed with the aid of a computer-linked television system which was used to define fringe positions relative to the fan coordinates and then calculate a deflection shape. The fringe order was determined by incrementing or decrementing, as appropriate, from the blade root and recognizing any inversion in the fringe count direction. An additional low contrast, widely spaced fringe set was present on some of the interferograms. This unexpected but useful feature was due to the presence during the recording of the hologram of a third laser pulse of low energy, which occurred a few hundred ns after one of the two main pulses. When present, this additional fringe set helped to confirm the fringe order.

The absolute axial displacement that occurred between the two laser pulses at a point can be calculated from the interferograms, by assuming that there is zero radial movement

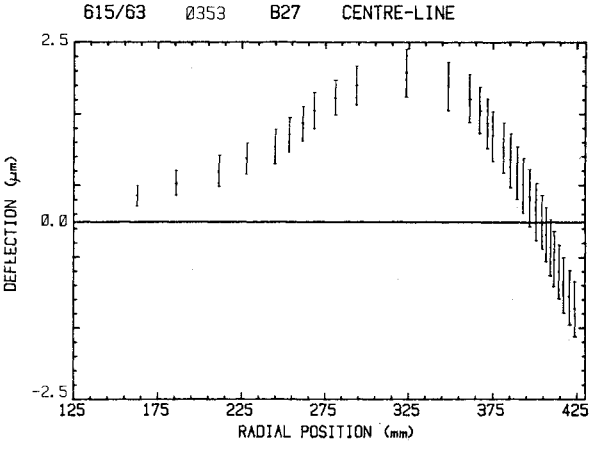

Fig. 15 Measured axial displacement along the centerline of a blade having minimal torsion at tip.

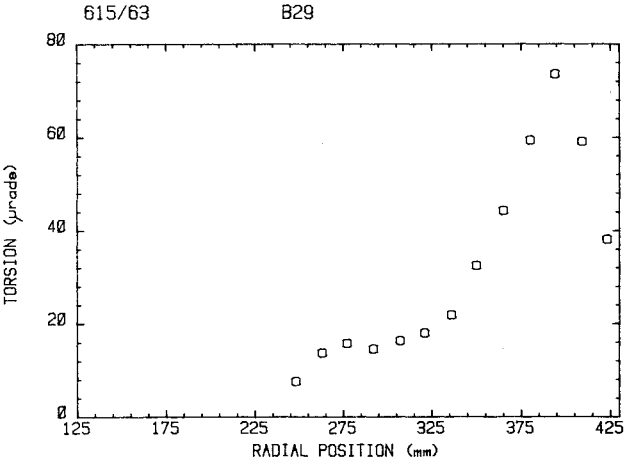

Fig. 16 Measured torsion as a function of radius for a blade having minimal axial displacement at tip.

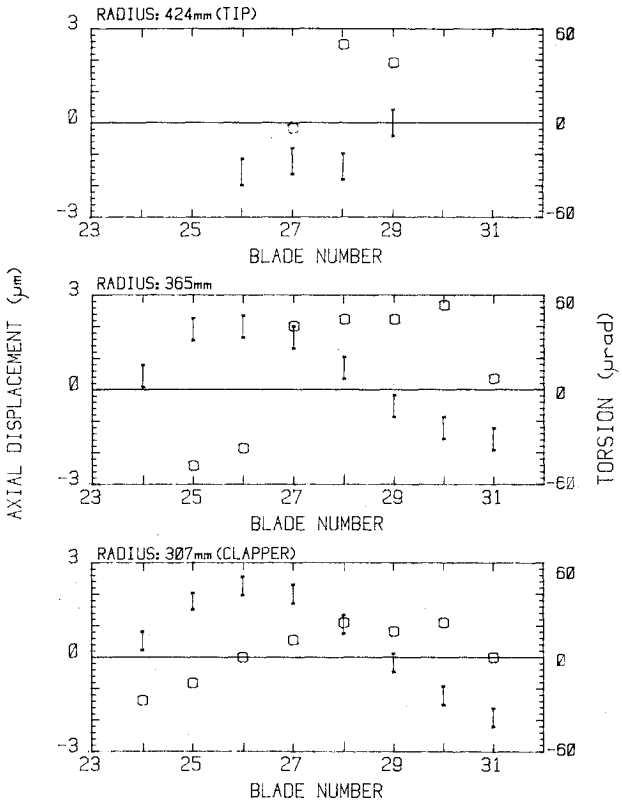

Fig. 17 Plots showing the circumferential distribution of torsion (*θ*) and centerline axial displacement (*I*).

and using the relationship,

$$F = (\boldsymbol{L} \cdot \boldsymbol{K})/\pi \tag{5}$$

where $\boldsymbol{F}$ is the fringe order, $\boldsymbol{L}$ the displacement vector, and $\boldsymbol{K}$ the holographic sensitivity vector, having magnitude $2\pi/\lambda$. Consideration of the geometry leads to the scalar relationship,

$$A = \frac{F\lambda}{2} \sec\left(\tan^{-1}\frac{r}{s}\right) \tag{6}$$

where A is the axial displacement that occurs between holographic exposures, λ the wavelength of light, r the radius of the point on the fan, and s the distance between the fan and the holographic system.

A measure of blade torsion T is obtained by calculating the angle at which a point on the leading edge rotates relative to the centerline. This is given by

$$T = 2(A_L - A_C)/(\sin(\delta)\, c) \tag{7}$$

where A_L and A_C are the axial displacements obtained at the leading edge and centerline, respectively, using Eq. (6), δ is the stagger angle of the blade, and c is the blade chord length. These are, generally, all variables of radial position.

By way of illustration, plots of blade torsion T and axial displacement A obtained from one interferogram are presented. This particular hologram was recorded at a fan speed of 9895 rpm using a pulse separation of 2 μs. A photographic negative of the interferogram recorded from the visual display of the computer-television analysis system is shown in Fig. 14. Superimposed on this interferogram is the fringe distribution along the centerline of a blade (No. 27) having minimal torsion at the tip. This fringe distribution was used to compute the plot of centerline axial displacement as a function of radius, shown in Fig. 15. Figure 16 is a plot of blade torsion as a function of radial position along blade 29, which was selected because it has minimal centerline displacement at the tip. There is considerable deviation in this plot of torsion from the expected distribution for the 3D2F mode. Plots of the circumferential distribution of torsion and centerline axial displacement, at three radii, are shown in Fig. 17. These plots also show some deviation from the sinusoidal distribution of torsion and bending, which would be expected. This is due to response of the blades in their individual modes of vibration, in addition to the 3D2F assembly mode. However, from Fig. 17, estimates of the spatial phase between torsion and axial displacement can be made; for instance, at the clapper this phase is approximately 90 deg, as would be expected. The error bars in Figs. 15 and 17 represent the uncertainty in the measurement due to the positional tolerance of the rotator with respect to the projected fan's axis. The average axial and angular velocities that occurred between the two laser pulses are obtained from the data shown in Figs. 15-17, by simply dividing the values of A and T by the pulse separation Δt. Thus, for instance, the average axial velocity at the tip of blade 27 was $1.2\times10^{-6}/2\times10^{-6} = 0.6\ \text{ms}^{-1}$, and the average angular velocity at the tip of blade 29 was $38\times10^{-6}/2\times10^{-6} = 19\ \text{rad s}^{-1}$.

Conclusions

This paper demonstrates the use of holographic interferometry to quantitatively determine the axial vibration over a large area of a fan rotating at approximately 10,000 rpm and undergoing unstalled supersonic flutter. In particular, the determination of the relative amplitude and phase of torsion and axial bending of the fluttering fan has been demonstrated. These are data to which a predicted flutter mode shape obtained, for example, by finite element analysis, can be compared. The determination of the distribution of torsion and bending is crucial for the modeling of a fan's flutter characteristics.[21,22]

Appendix – Expression for Bias Fringe Field

An expression is derived for the bias fringe field generated by misalignment of the image rotator relative to the fan's axis. The stationary coordinate system and geometrical configuration are shown in Fig. 12. For simplicity, the source of illumination and the collection aperture are approximated to coincident points on the rotator axis at Q, having coordinates x_Q, y_Q, z_Q. P_1 is a general point on the fan at x_1, y_1, z_1, at the time of the first exposure. Rotation of the fan of $\Delta\theta$ between exposures moves this point to P_2 at x_2, y_2, z_2. The rotation of the rotator serves to maintain correlation between the two images of the fan, but does not introduce any pathlength change. Thus, the total pathlength change is $2(P_2Q - P_1Q)$. This will introduce an error of m full fringes in the resultant interferogram, given by

$$m = (2/\lambda)\ (P_2Q - P_1Q) \tag{A1}$$

where λ is the wavelength of light. From the geometry,

$$(P_KQ)^2 = (x_Q - x_K)^2 + (y_Q - y_K)^2 + (z_Q - z_K)^2 \quad \text{for } K = 1,2 \tag{A2}$$

$$(P_KQ)^2 = (x_Q - r\cos\theta_K)^2 + (y_Q - r\sin\theta_K)^2 + (z_Q - z_K)^2 \quad \text{for } K = 1,2 \tag{A3}$$

where $r = 0P_1 = 0P_2$ and θ_1, θ_2 are defined in Fig. 12.

From an expansion of Eq. (A3) and using $z_1 = z_2$,

$$(P_2Q)^2 - (P_1Q)^2 = 2x_Qr(\cos\theta_1 - \cos\theta_2) + 2y_Qr(\sin\theta_1 - \sin\theta_2) \tag{A4}$$

Assuming small $\Delta\theta = \theta_2 - \theta_1$ and letting $\theta = \theta_1$,

$$(P_2Q)^2 - (P_1Q)^2 \cong 2\Delta\theta x_Q \, r\sin\theta - 2\Delta\theta y_Q \, r\cos\theta \qquad \text{(A5)}$$

Let $x_p = x_1$ and $y_p = y_1$

$$(P_2Q)^2 - (P_1Q)^2 \cong 2\Delta\theta \, (x_Q y_p - y_Q x_p) \qquad \text{(A6)}$$

$$P_2Q - P_1Q \cong \frac{(P_2Q)^2 - (P_1Q)^2}{P_2Q + P_1Q} \qquad \text{(A7)}$$

For small misalignments, $P_2Q + P_1Q \cong 2\ell$, thus

$$P_2Q - P_1Q \cong \frac{\Delta\theta}{\ell} \, (x_Q y_p - y_Q x_p) \qquad \text{(A8)}$$

Thus from Eq. A1,

$$m \cong \frac{2\Delta\theta}{\lambda\ell} \, (x_Q y_p - y_Q x_p) \qquad \text{(A9)}$$

Acknowledgments

This work was supported by the Ministry of Defence (Procurement Executive). The author gratefully acknowledges Rolls-Royce Ltd. for permission to publish this paper. The author also wishes to thank colleagues in the Advanced Research Laboratory and Aeroelastic Group who have assisted in carrying out this work and, in particular, D. G. Jones for his advice and encouragement.

References

[1] Hockley B. S., Ford, R. A. J. and Foord, C. A., "Measurement of Fan Vibration Using Double Pulsed Holography," *ASME Transactions, Journal of Engineering for Power,* Vol. 100, Oct. 1978, pp. 655-663.

[2] Stetson, K. A. and Harrison, I. R., "Computer-Aided Holographic Vibration Analysis for Vectorial Displacements of Bladed Disks," *Applied Optics,* Vol. 17, June 1978, pp. 1733-1738.

[3] Waddell, A. J., Kennedy, W., and Waddell, P., "Vibration Analysis for Static and Rotating Objects by Stroboscopic Holography," *Proceedings of the International Symposium on Holography,* Besancon, France, July 1970, Co-sponsored by Commision International d'Optique and Comité Francais d'Optique, Paper 6-6.

[4] Kawase, S., Honda, T., and Tsujiuchi, J., "Measurement of Elastic Deformation of Rotating Objects by Using Holographic Interferometry," *Optics Communications,* Vol. 16, Jan. 1976, pp. 96-98.

[5] Tsuruta, T. and Itoh Y., "Holographic Interferometry for Rotating Subject," *Applied Physics Letters,* Vol. 17, July 1970, pp. 85-87.

[6] Sikora, J. P., and Mendenhall, F. T., "Holographic Vibration Study of a Rotating Propeller Blade," *Experimental Mechanics,* Vol. 14, June 1974, pp. 230-232.

[7] Beeck, M. A., and Kreitlow, H., "Conditions and Examinations of Vibration Analysis of Rotating Blades with the Help of Holographic Interferometry," *Laser 77 Opto-Electronics Conference Proceedings,* Munich, Germany, June 1977, IPC Science and Technology Press, pp. 408-419.

[8] Stetson, K. A., "The Use of an Image Derotator in Hologram Interferometry and Speckle Photography of Rotating Objects," *Experimental Mechanics,* Vol. 18, Feb. 1978, pp. 67-73.

[9] Erf, R. K., and Stetson K. A., "The Dynamic Analysis of Rotating Structures with Holographic Interferometry," AIAA Paper 80-1142, July 1980.

[10] MacBain, J. C., Horner, J. E., Stange, W. A., and Ogg, J. S., "Vibration Analysis of a Spinning Disk Using Image Derotated Holographic Interferometry," *Experimental Mechanics,* Vol. 19, Jan. 1979, pp. 17-22.

[11] Clarady, J. F., and Bearden, J. L., "Spin Rig Applications of Image Derotated Holographic Interferometry," Topical Meeting on Hologram Interferometry and Speckle Metrology, Cape Cod, Mass., Optical Society of America, June 1980.

[12] MacBain, J. C., Stange, W. A., and Harding, K. G., "Real-Time Response of a Rotating Disk Using Image Derotated Holographic Interferometry," *Experimental Mechanics,* Vol. 21, Jan. 1981, pp. 34-40.

[13] MacBain J. C., Stange, W. A., and Harding, K.G., "Analysis of Rotating Structures Using Image Derotation with Multiple Pulsed Lasers and Moiré Techniques," SESA Spring 1981 Meeting, Detroit, Michigan.

[14] Stange, W. A., and MacBain, J. C., "An Investigation of Duel Mode Phenomena In a Mistuned Bladed Disk," ASME Paper 81-DET-133, Sept. 1981.

[15] Beeck, M. A., and Fagan, W. F., "Study of the Dynamic Behavior of Rotating Automobile Fans Using Image Derotated Holographic Interferometry," Topical Meeting on Hologram Interferometry and Speckle Metrology, Cape Cod, Mass., Optical Society of America, Paper WA2, June 1980.

[16] Fagan, W. F., Beeck, M. A., and Kreitlow, H., "The Holographic Vibration Analysis of Rotating Objects Using a Reflective Image Derotator," *Optics and Lasers in Engineering,* Vol. 2, Jan. 1981, pp. 22-32.

[17] MacBain, J. C., "Hologram Interferometry of Rotating Structures," Topical Meeting on Hologram Interferometry and Speckle Metrology, Cape Cod, Mass., Optical Society of America, Paper WA1, June 1980.

[18] Swift, D. W., "Image Rotation Devices—a Comparative Survey," *Optics and Laser Technology,* Vol. 4, Aug. 1972, pp. 175-188.

[19] Den Hartog, J. P., *Mechanical Vibrations,* McGraw Hill Book Co. Inc., New York, 1934, pp. 276-289.

[20] Koechner, W., *Solid-State Laser Engineering,* Springer-Verlag, 1976, pp. 212-217.

[21] Carta, F. O., "Coupled Blade-Disk Shroud Flutter Instabilities in Turbojet Engine Rotors," *ASME Transactions, Journal of Engineering for Power,* Vol. 89, July 1967, pp. 419-426.

[22] Halliwell, D. G., "The Characteristics Prediction and Test Analysis of Supersonic Flutter in Turbofan Engines," I Mech E, Paper C187/76, Conference on Vibrations in Rotating Machinery, Sept. 1976.